Super-convergence Analysis on two symmetric Poisson solvers in Octree grids

Byungjoon Lee*, Jeongho Kim†and Chohong Min‡

January 10, 2022

Abstract

The Hodge decomposition, that is an important feature of incompressible fluid flows, is orthogonal and the projection taking its incompressible component is therefore stable. The decomposition is implemented by solving the Poisson equation. In order to simulate incompressible fluid flows in a stable manner, it is desired to utilize a Poisson solver that attains the orthogonality of the Hodge decomposition in a discrete level.

When a Poisson solver induces the orthogonality, its associated linear system is necessarily symmetric. With this regard, the symmetric Poisson solvers [9, 8] by Losasso et al. are more advantageous not only to efficiently solving the linear system but also to stably simulating fluid flows than nonsymmetric ones. Their numerical solutions were empirically observed to be first and second order accurate, respectively. One may expect that each of their numerical gradients has convergence order that is one less than that of its numerical solution.

However, we in this work show that super-convergence holds true with both Poisson solvers. Rigorous analysis is presented to prove that the difference is one half, not one between the convergence orders of numerical solution and gradient in both solvers. The analysis is then validated with numerical results. We furthermore show that both Poisson solvers, being symmetric, indeed satisfy the orthogonal property in the discrete level and yield stable implementations of the Hodge decomposition in octree grids.

1 Introduction

Physical phenomena in many cases are multi-scaled. To efficiently resolve its small scales, it is requested to adopt adaptive grids that can allocate more computational resources to the regions of smaller scales. Octree grid achieves the adaptivity by just recursively splitting cells containing the small scales. The grid generation is very fast and efficient, compared to triangular meshes. However, in octree grids, two neighboring cells may differ in their sizes and do not share the common face, giving rise to T-junctions. The presence hindered the progress of efficient Poisson solvers in octree grids. Compared to the long history of finite element methods [7, 15] on triangular meshes, it is quite recent to see some on octree. Popinet [11] introduced a second order accurate method and Min et al. another one with smaller numerical support [10]. The associated linear system of each method is nonsymmetric.

Losasso et al. [9] introduced a symmetric method on octree grids whose numerical solution is first order accurate. Later on, they enhanced the first order accuracy to the second order [8] while maintaining the symmetry. We note that symmetric methods are more advantageous not only to efficiently solving the linear systems but also to stably simulating incompressible fluid flows than nonsymmetric ones. The Poisson equation has many equivalent formulations, among which we pay attentions to the formulation that characterizes its solution as the minimizer of an L^2 energy [1]. The energy minimization is related to the stability of Hodge projection that plays an important role in incompressible fluid flows. While the analytic solution of the Poisson equation is the minimizer of the energy, a numerical solution of the equation may not be the minimizer in discrete level. To yield robust and reliable simulations of incompressible fluid flows, a numerical solution is desired to also satisfy the minimization property. A necessary condition of the minimization property is that the associated linear system is symmetric.

A main object of this study is that the two symmetric Poisson solvers indeed satisfy the minimization property. As a consequence, the Hodge projection induced by each of them is stable. Another main object is to present

*Department of Mathematics, The Catholic University of Korea, South Korea
†Research Institute for Natural Sciences, Hanyang University, South Korea
‡Department of Mathematics, Ewha Womans University, South Korea

and prove the super-convergence for each solver. Usually, a numerical gradient has convergence order that equals the convergence order of its corresponding numerical solution minus one. However, in solving elliptic problems with uniform or nearly uniform grid cells [6], the order of the gradient may not drop to the usual order, so called super-convergence. In octrees, the order of accuracy is measured sequentially, starting from an arbitrary octree and splitting all the leaf cells. In the measurements, there can be many levels, but the cells of each level are of the same size. We found out that super-convergence occurs in each of the two methods and provide in this work a rigorous analysis for the super-convergences.

A conventional anaylsis [3, 14] for Poisson solvers with Dirichlet boundary conditions first measures their errors near the boundary, and then moves on to inside estimation using maximum principle and Perron-Frobenius theorem [13]. In the case of Neumann boundary conditions, with which the two symmetric Poisson solvers are imposed, there is no place in which the error is a priori known. In our earlier work [16], we proved a super-convergence of Purvis-Burkhalter method [12] that deals with Neumann boundary conditions. A key idea in the work is to represent consistency error as an image of divergence operator and use discrete symmetries.

We continue with the earlier research in this study to prove the super-convergences of the two symmetric Poisson solvers. Numerical gradient and divergence operators are defined, and their symmetries or integration-by-parts are shown. The consistency error of the first order method is represented as an image of divergence, and then the numerical gradient of the first order method is shown to be $1/2$ order accurate. Up to this point, the study has almost a word-to-word correspondence to the earlier research. However, the super-convergence of the second order method cannot be proved by the eariler methodology alone, posing a new challange. The second order method ingeniusly employs an averaging operator on the first order method. The L^2 norm of the average operator is less than or equal to one. The norm estimation of the operator in the reverse direction turned out to be crucial to proving the super-convergence of the second order method.

This article consists of five sections. The second and third sections introduce mathematical analyses on the two Poisson solvers, and numerical results in the fourth section validate the analyses. In specific, section 2.1 defines three numerical operators by which the two solvers are briefly formulated. The symmetry relations between the numerical operators are reported and proved in section 2.2. Both solvers are shown in section 2.3 to satisfy the L^2-minimization and consequently induce stable Hodge projections. Section 3 begins with representing and estimating their consistency errors as the images of numerical divergence. The section then introduces the norm estimation in the reverse direction and proves the super-convergences of the two methods. Some theorems entail very lengthy proofs, which were put in the appendix.

2 Symmetric Poisson Solvers in quad/octrees

In this section, we first define three numerical operators in quad/octrees, by which the two symmetric Poisson solvers are efficiently formulated. We then show the symmetries of the numerical operators, through which the two solvers are shown to satisfy the minimization principle [1]. Furthermore, the Hodge decomposition induced by each of the solvers is shown to be stable.

2.1 Numerical operators

Figure 1 (left) depicts the MAC configuration, where pressure is sampled at each cell center and velocity components at cell faces. In Figure 1 (right), A_{ij} denotes the face between two adjacent cells C_i and C_j, and its control volume is the rectangle of size $\triangle_{ij} \times |A_{ij}|$. Given a pressure variable p defined at cell centers, numerical gradient G^h defines a variable $G^h p$ at cell faces as

$$(G^h p)_{ij} = \pm \frac{p_j - p_i}{\triangle_{ij}} = \sigma_{ij} \frac{p_j - p_i}{\triangle_{ij}}, \tag{1}$$

where $\sigma_{ij} = (1,1) \cdot n_{ij}$ marks the direction of the outward unit normal vector n_{ij} of the cell C_i at the face A_{ij}. Conversely, given a velocity variable f at cell faces, numerical divergence D^h defines a variable $D^h f$ at cell centers as

$$(D^h f)_i = \sum_{C_i \sim C_j} f_{ij} \, |A_{ij}| \, \sigma_{ij}, \tag{2}$$

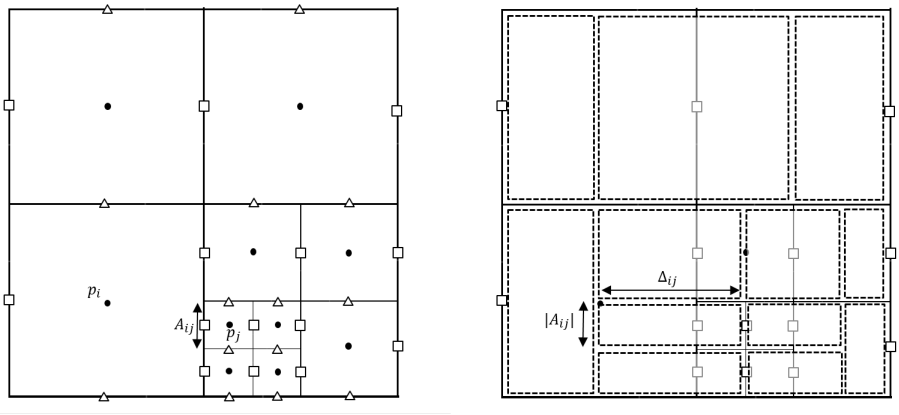

Figure 1: The MAC configuration in quadtree (left) and the control volumes ($\Delta_{ij} \times |A_{ij}|$) of faces A_{ij} fill the domain without any overlap (right).

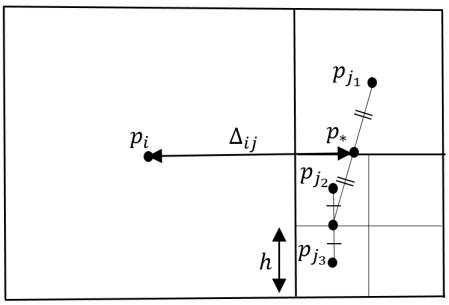

Figure 2: $\frac{p_{j_k}-p_i}{\Delta_{j_k i}}$ is not approximating $\frac{\partial p}{\partial x}$ at all, for $k = 1, 2, 3$. However, $\frac{p_*-p_i}{\Delta_{ij}}$ is approximating the derivative with the first order accuracy.

where the summation runs over all the cells C_j adjacent to C_i. Utilizing numerical gradient and divergence operators, the first-order Poisson solver is formulated as

$$D^h G^h p^h_{1st} = D^h U^{*,h}, \tag{3}$$

where $U^{*,h} := \sigma_{ij}(U^*_{ij} \cdot n_{ij})$. It approximates the following Poisson equation with Neumann boundary conditions in a rectangular domain Ω.

$$\begin{cases} \Delta p = \nabla \cdot U^* & \text{in } \Omega \\ \frac{\partial p}{\partial n} = U^* \cdot n & \text{on } \partial\Omega \end{cases} \tag{4}$$

To enhance the order of accuracy, the authors in [8] noted that the convergence order of the numercial gradient is merely zero whenever two adjacent cells differ in sizes, and could increase the order by taking an weighted sum on numerical gradients. For example, the cells C_{j_1},C_{j_2}, C_{j_3} in Figure 2 are not horizontally aligned with C_i, which causes the inaccuracy of $(G^h p)_{ij_1}$, $(G^h p)_{ij_2}$, $(G^h p)_{ij_3}$. As illustrated in the figure, a recursive averaging on the small cells can make it aligned:

$$\frac{p_{j_1} + \frac{p_{j_2}+p_{j_3}}{2}}{2} - p_i}{\triangle_{ij}} = \frac{\partial p}{\partial x} + O(h).$$

The recursive averaging on p_{j_1},p_{j_2},p_{j_3} can be cast into a weighted average on $(G^h p)_{ij_1}$,$(G^h p)_{ij_2}$, $(G^h p)_{ij_3}$ as follows:

$$\frac{\frac{p_{j_1}+\frac{p_{j_2}+p_{j_3}}{2}}{2}-p_i}{\triangle_{ij}} = \frac{\frac{p_{j_1}-p_i}{\triangle_{ij_1}}\cdot\triangle_{ij_1}|A_{ij_1}| + \frac{p_{j_2}-p_i}{\triangle_{ij_2}}\cdot\triangle_{ij_2}|A_{ij_2}| + \frac{p_{j_3}-p_i}{\triangle_{ij_3}}\cdot\triangle_{ij_3}|A_{ij_3}|}{\triangle_{ij_1}|A_{ij_1}| + \triangle_{ij_2}|A_{ij_2}| + \triangle_{ij_3}|A_{ij_3}|}$$
$$= \left(\sum_k (Gp)_{ij_k}\triangle_{ij_k}|A_{ij_k}|\right) / \left(\sum_k \triangle_{ij_k}|A_{ij_k}|\right).$$

For a velocity field f defind at call faces, the weighted averaging, denoted by W^h, defines $W^h f$ again at cell faces as

$$\left(W^h f\right)_{ij_l} = \frac{\sum_k f_{ij_k}\triangle_{ij_k}|A_{ij_k}|}{\sum_k \triangle_{ij_k}|A_{ij_k}|}, \tag{5}$$

for each l. When C_i and C_j are of the same size, $(W^h f)_{ij} = f_{ij}$. Utilizing the weighted averaging W^h on the gradient, the second-order method is simply formulated as

$$D^h W^h G^h p^h_{2nd} = D^h W^h U^{*,h}. \tag{6}$$

2.2 Symmetries

The three numerical operators are related to each other through some symmetries. For example, numerical gradient is a negative adjoint of numerical divergence, and vice versa. Moreover, the weighted averaging is self-adjoint. To show the adjoint or symmetry relations, we impose inner product structure on quad/octree. For velocity fields f_1 and f_2 sampled at cell faces, their inner product, using the control volume $\triangle_{ij}\times|A_{ij}|$, of face A_{ij} is defined as

$$\langle f_1, f_2\rangle_F = \sum_{A_{ij}} (f_1)_{ij}\,(f_2)_{ij}\,\triangle_{ij}\,|A_{ij}|\,.$$

For pressure variables sampled at cell centers, their inner product needs to be defined in the same way using the control volume of each cell. Numerical divergence (2) was defined as the net sum of fluxes, based on the divergence theorem $\int_{C_i}\nabla\cdot f dv = \int_{\partial C_i} f\cdot n d\Gamma$. Numerical divergence with this regard includes the control volume of each cell. Thus for pressure p and divergence $D^h f$, their inner product is defined as

$$\left\langle p, D^h f\right\rangle_C = \sum_{C_i} p_i\left(D^h f\right)_i.$$

The following two lemmas show the adjoint relation and symmetry of the numerical operators. The first one is for the adjoint relation between D^h and G^h, and the second is for the self-adjointness of W^h.

Lemma 1 (Adjoint relation between D^h and G^h)**.** *Let $c=\{c_i\}$ and $f=\{f_{ij}\}$ be two vectors defined on the center of cells and faces respectively. Then, we have $\langle D^h f, c\rangle_C = -\langle f, G^h c\rangle_F$.*

Proof. We use the definitions of the numerical operators to observe that

$$\begin{aligned}\langle D^h f, c\rangle_C = \sum_{C_i}(D^h f)_i c_i &= \sum_{C_i}\sum_{C_j\sim C_i} f_{ij}|A_{ij}|\sigma_{ij}c_i = \sum_{A_{ij}} f_{ij}|A_{ij}|(\sigma_{ij}c_i+\sigma_{ji}c_j)\\ &= -\sum_{A_{ij}} f_{ij}\left(\frac{c_j-c_i}{\Delta_{ij}}\sigma_{ij}\right)\Delta_{ij}|A_{ij}|\\ &= -\sum_{A_{ij}} f_{ij}(G^h c)_{ij}\Delta_{ij}|A_{ij}| = -\langle f, G^h c\rangle_F,\end{aligned}$$

where we used $\sigma_{ij}=-\sigma_{ji}$. Therefore, the desired adjoint relation holds. □

Next, we show that the weighted averaging operator W^h is a symmetric projection operator.

Lemma 2 (Self-adjointness of W^h)**.** *Let $f = \{f_{ij}\}$ and $g = \{g_{ij}\}$ are two vectors defined on the cell faces. Then, we have $(W^h)^2 = W^h$ and $\langle W^h f, g\rangle_F = \langle f, W^h g\rangle_F$.*

Proof. Since W^h is a weighted averaging operator, it is clear that $(W^h)^2 = W^h$. Moreover, W^h is a local operator in the sense that f_{ij} can only affect the components of $W^h f$ at the face that share a common large cell with A_{ij}. Therefore, it is enough to show that W^h is symmetric on a single large cell face. Consider the structure depicted in Figure 2 for simplicity. It follows from the definition of W^h that $(W^h f)_{ij_1} = (W^h f)_{ij_2} = (W^h f)_{ij_3}$ and therefore, we have

$$\begin{aligned}
&(W^h f)_{ij_1} g_{ij_1} \Delta_{ij_1} |A_{ij_1}| + (W^h f)_{ij_2} g_{ij_2} \Delta_{ij_2} |A_{ij_2}| + (W^h f)_{ij_3} g_{ij_3} \Delta_{ij_3} |A_{ij_3}| \\
&= (W^h f)_{ij_1} \left(g_{ij_1} \Delta_{ij_1} |A_{ij_1}| + g_{ij_2} \Delta_{ij_2} |A_{ij_2}| + g_{ij_3} \Delta_{ij_3} |A_{ij_3}| \right) \\
&= \frac{f_{ij_1} \Delta_{ij_1} |A_{ij_1}| + f_{ij_2} \Delta_{ij_2} |A_{ij_2}| + f_{ij_3} \Delta_{ij_3} |A_{ij_3}|}{\Delta_{ij_1} |A_{ij_1}| + \Delta_{ij_2} |A_{ij_2}| + \Delta_{ij_3} |A_{ij_3}|} \left(g_{ij_1} \Delta_{ij_1} |A_{ij_1}| + g_{ij_2} \Delta_{ij_2} |A_{ij_2}| + g_{ij_3} \Delta_{ij_3} |A_{ij_3}| \right) \\
&= \left(f_{ij_1} \Delta_{ij_1} |A_{ij_1}| + f_{ij_2} \Delta_{ij_2} |A_{ij_2}| + f_{ij_3} \Delta_{ij_3} |A_{ij_3}| \right) \frac{g_{ij_1} \Delta_{ij_1} |A_{ij_1}| + g_{ij_2} \Delta_{ij_2} |A_{ij_2}| + g_{ij_3} \Delta_{ij_3} |A_{ij_3}|}{\Delta_{ij_1} |A_{ij_1}| + \Delta_{ij_2} |A_{ij_2}| + \Delta_{ij_3} |A_{ij_3}|} \\
&= f_{ij_1} (W^h g)_{ij_1} \Delta_{ij_1} |A_{ij_1}| + f_{ij_2} (W^h g)_{ij_2} \Delta_{ij_2} |A_{ij_2}| + f_{ij_3} (W^h g)_{ij_3} \Delta_{ij_3} |A_{ij_3}|.
\end{aligned}$$

Therefore, the weighted averaging operator W^h is a symmetric operator. □

2.3 Stable Hodge decompositions

For a velocity field U^*, the numerical solution p^h_{1st} is used to define $U^h_{1st} := U^{*,h} - G^h p^h_{1st}$ and obtain Hodge decomposition

$$U^{*,h} = U^h_{1st} + G^h p^h_{1st} \text{ with } D^h U^h_{1st} = 0.$$

Similarly, p^h_{2nd} is used to define $U^h_{2nd} := U^{*,h} - W^h G^h p^h_{2nd}$ and obtain

$$U^{*,h} = U^h_{2nd} + W^h G^h p^h_{2nd} \text{ with } D^h W^h U^h_{2nd} = 0.$$

The following two propositions show that each of the above decompositions is stable. Since the proofs are almost identical, we only provide the proof for the second-order method.

Proposition 3. *The numerical solution p^h_{1st} is a minimizer of the following energy functional*

$$E^h_{1st}(p^h) := \frac{1}{2} \|G^h p^h\|^2_F - \langle G^h p^h, U^{*,h} \rangle_F.$$

In particular, we have $\|U^h_{1st}\|_F \le \|U^{*,h}\|_F$.

Proposition 4. *The numerical solution p^h_{2nd} is a minimizer of the following energy functional*

$$E^h_{2nd}(p^h) := \frac{1}{2} \|W^h G^h p^h\|^2_F - \langle W^h G^h p^h, U^{*,h} \rangle_F.$$

In particular, we have $\|U^h_{2nd}\|_F \le \|U^{*,h}\|_F$.

Proof. For any perturbation $q^h = \{q^h_i\}$, we use symmetry of W^h and adjoint relation between D^h and G^h to estimate $E^h_{2nd}(p^h_{2nd} + q^h)$ as

$$\begin{aligned}
E^h_{2nd}(p^h_{2nd} + q^h) &= \frac{1}{2} \|W^h G^h (p^h_{2nd} + q^h)\|^2_F - \langle W^h G^h (p^h_{2nd} + q^h), U^{*,h} \rangle_F \\
&= E^h_{2nd}(p^h_{2nd}) + \langle W^h G^h q^h, W^h G^h p^h_{2nd} \rangle_F + \frac{1}{2} \|W^h G^h q^h\|^2_F - \langle W^h G^h q^h, U^{*,h} \rangle_F \\
&= E^h_{2nd}(p^h_{2nd}) + \frac{1}{2} \|G^h q^h\|^2_F \ge E^h_{2nd}(p^h_{2nd}),
\end{aligned}$$

where we used $D^h W^h G^h p^h_{2nd} = D^h W^h U^{*,h}$. Therefore, p^h_{2nd} is a minimizer of the energy functional E^h_{2nd}. In particular, we obtain $E^h_{2nd}(p^h_{2nd}) \le E^h_{2nd}(0)$, which implies

$$\frac{1}{2}\|U^{*,h} - U^h_{2nd}\|^2_F - \langle U^{*,h} - U^h_{2nd}, U^{*,h}\rangle_F \le 0, \quad \text{i.e.,} \quad \|U^h_{2nd}\|_F \le \|U^{*,h}\|_F.$$

□

3 Super-convergences

It is usual that numerical gradient has the order of accuracy that equals the order of numerical solution minus one. However, in the case of solving elliptic problems in grid cells that are uniform or nearly uniform, the order of gradient may not lose the one in the order, which is so-called super-convergence. In this section, we introduce and prove the super-convergence for each of the two numerical solutions.

To compare the analytic solution to the numerical solutions, we introduce an averaging operator S^h. For a continuous vector field $U : \mathbb{R}^d \to \mathbb{R}^d$ (d=2,3), $S^h U$ is the velocity field at cell faces defined as

$$(S^h U)_{ij} := \frac{\sigma_{ij}}{|A_{ij}|}\int_{A_{ij}} U \cdot n_{ij} d\Gamma.$$

Applying the Gauss-Green formula to $U = U^* - \nabla p$ that is divergence free, we get on each cell C_i that

$$\begin{aligned} 0 = \int_{C_i} \nabla \cdot U \, dV &= \sum_{C_j \sim C_i} \int_{A_{ij}} U \cdot n_{ij} \, d\Gamma \\ &= \sum_{C_j \sim C_i} \sigma_{ij} \, |A_{ij}| \left(S^h U\right)_{ij} \\ &= \left(D^h S^h U\right)_i, \end{aligned}$$

or

$$D^h S^h \nabla p = D^h S^h U^*. \tag{7}$$

Let us define error vectors $e^h_{1st} := p^h_{1st} - p$ and $e^h_{2nd} := p^h_{2nd} - p$. Combining (3) and (7) leads to

$$\begin{aligned} D^h G^h e^h_{1st} &= D^h G^h p^h_{1st} - D^h G^h p \\ &= D^h U^* - D^h G^h p \\ &= D^h \left(U^* - S^h U^* - G^h p + S^h \nabla p\right) \\ &=: D^h d^h_{1st}. \end{aligned}$$

Similarly, combining (6) and (7) leads to

$$\begin{aligned} D^h W^h G^h e^h_{2nd} &= D^h \left(W^h U^* - S^h U^* - W^h G^h p + S^h \nabla p\right) \\ &=: D^h d^h_{2nd}. \end{aligned}$$

The consistency errors d^h_{1st} and d^h_{2nd} do not involve numerical solutions and can be estimated in terms of the analytic solutions p and U^* according to the types of faces. If the cells C_i and C_j are the same size, then the face A_{ij} is said to be uniform. Otherwise, A_{ij} is said to be non-uniform.

Lemma 5. *The consistency error $d^h_{1st} = \{d^h_{1st,ij}\}$ is estimated as*

$$|d^h_{1st,ij}| \le \begin{cases} C_1 h^2, & \text{if } A_{ij} \text{ is uniform,} \\ C_2, & \text{if } A_{ij} \text{ is non-uniform} \end{cases}$$

where h denotes the size of the largest cell and C_1 and C_2 are constants depending only on U^* and p.

Lemma 6. *The consistency error $d^h_{2nd} = \{d^h_{2nd,ij}\}$ is estimated as*

$$|d^h_{2nd,ij}| \le \begin{cases} C_1 h^2, & \text{if } A_{ij} \text{ is uniform,} \\ C_2 h, & \text{if } A_{ij} \text{ is non-uniform} \end{cases}$$

where h denotes the size of the largest cell and C_1 and C_2 are constants depending only on U^* and p.

We present the detailed proof for Lemma 6 in Appendix, whereas the proof of Lemma 5 is omitted, since it can be proven in a similar manner. Utilizing $D^h\left(d^h_{1st} - G^h e^h_{1st}\right) = 0$ and the adjoint relation in Lemma 1, we get that $d^h_{1st} - G^h e^h_{1st}$ is orthogonal to $G^h e^h_{1st}$. Applying the Pythagorean theorem, we have

$$\begin{aligned} \left\|d^h_{1st}\right\|^2_F &= \left\|d^h_{1st} - G^h e^h_{1st}\right\|^2_F + \left\|G^h e^h_{1st}\right\|^2_F \\ &\ge \left\|G^h e^h_{1st}\right\|^2_F, \end{aligned}$$

and simply proved the following theorem.

Theorem 7 (Super-convergence of $G^h p^h_{1st}$)**.** *For a given function $U^* : \Omega \to \mathbb{R}^2$ (or $\mathbb{R}^3$), let p be a solution to the 2-D (or 3-D) Poisson equation (4), and let p^h_{1st} be the numerical solution of the first-order method (3). Then, the discrete gradient has a half-order convergence in discrete L^2-norm:*

$$\|G^h(p^h_{1st} - p)\|_F \le Ch^{1/2}.$$

Proof. We first consider two-dimensional quadtree case, and discuss about the octree case at the end of proof. It is enough to show that $\|d^h_{1st}\|^2_F$ is bounded by $C^2 h$ for some constant C. We use Lemma 5 to obtain

$$\begin{aligned} \|d^h_{1st}\|^2_F &= \sum_{A_{ij}:\text{uniform}} |d^h_{1st,ij}|^2 \Delta_{ij} |A_{ij}| + \sum_{A_{ij}:\text{non-uniform}} |d^h_{1st,ij}|^2 \Delta_{ij} |A_{ij}| \\ &\le C_1^2 h^6 (\#\text{ of uniform faces}) + C_2^2 h^2 (\#\text{ of non-uniform faces}). \end{aligned}$$

However, the number of uniform faces and non-uniform faces are bounded by

$$(\#\text{ of uniform faces}) \le C_3 h^{-2}, \quad (\#\text{ of non-uniform faces}) \le C_4 h^{-1},$$

where C_3 and C_4 are the constants only depend on the initial quadtree structure. Therefore, we estimate the L^2-norm of d^h_{1st} as

$$\|d^h_{1st}\|^2_F \le C_1^2 C_3 h^4 + C_2^2 C_4 h \le C^2 h, \tag{8}$$

for sufficiently small h, where $C = \sqrt{2C_2^2 C_4}$. This yields the desired half order convergence of the discrete gradient. In the octree case, we have $\Delta_{ij} |A_{ij}| \le h^3$, while the number of uniform faces and non-uniform faces are bounded by

$$(\#\text{ of uniform faces}) \le C_3 h^{-3}, \quad (\#\text{ of non-uniform faces}) \le C_4 h^{-4}.$$

Therefore, the estimate (8) still valids. □

The second order case is not as simple as the first order, mainly becase $W^h d^h_{2nd} \ne d^h_{2nd}$. We use the adjoint relations and the projection property $\left(W^h\right)^2 = W^h$ to have

$$\begin{aligned} \|d^h_{2nd}\|^2_F &= \|d^h_{2nd} - W^h G^h e^h_{2nd}\|^2_F + \|W^h G^h e^h_{2nd}\|^2_F + 2\langle d^h_{2nd} - W^h G^h e^h_{2nd}, W^h G^h e^h_{2nd}\rangle_F \\ &= \|d^h_{2nd} - W^h G^h e^h_{2nd}\|^2_F + \|W^h G^h e^h_{2nd}\|^2_F + 2\langle d^h_{2nd}, W^h G^h e^h_{2nd} - G^h e^h_{2nd}\rangle_F \\ &= \|d^h_{2nd} - W^h G^h e^h_{2nd}\|^2_F + \|W^h G^h e^h_{2nd}\|^2_F + 2\langle W^h d^h_{2nd} - d^h_{2nd}, G^h e^h_{2nd}\rangle_F. \end{aligned} \tag{9}$$

To derive an estimate for the second term of the right-hand side of (9), we show that the L^2-norm of $G^h e^h_{2nd}$ can be controlled by the L^2-norm of $W^h G^h e^h_{2nd}$.

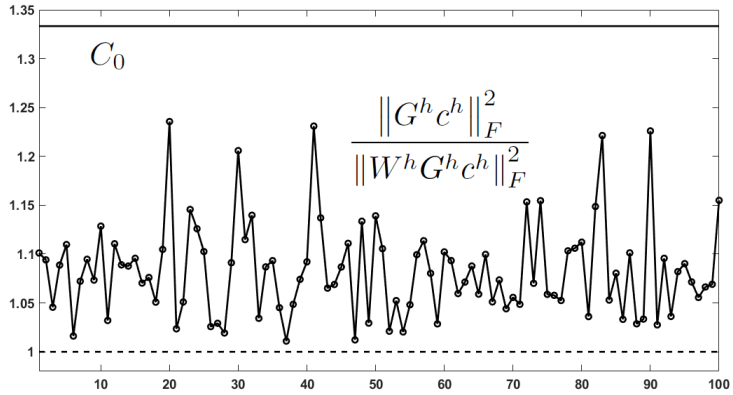

Figure 3: Plots of the ratio $\left\|G^h c^h\right\|_F^2 / \left\|W^h G^h c^h\right\|_F^2$ for the random vector c^h, the constant C_0 in the lemma 8, and the number 1. The effective resolution for the example is set to be four by splitting the bottom-left and top-right grids of the original grid configuration so that the constant C_0 is 4/3, from table 3. The results show that the ratio $\left\|G^h c^h\right\|_F^2 / \left\|W^h G^h c^h\right\|_F^2$ is bounded below by 1 and above by C_0 for any vector c^h, which demonstrate the result of lemma 8.

Lemma 8 (L^2 estimate of W^h)**.** *For any vector $c^h = \{c_i^h\}$ defined on the centers of cells, there exists a positive constant C_0 such that $\|W^h G^h c^h\|_F^2 \le \|G^h c^h\|_F^2 \le C_0 \|W^h G^h c^h\|_F^2$. Here, the constant C_0 only depends on the grid structure, not depending on h.*

Numerical results for 100 random vectors c^h in figure 3 validate the lower and upper bounds in lemma 8. Thanks to Lemma 8, we are now able to close the estimate (9) and yield the following theorem.

Theorem 9 (Super-convergence of $W^h G^h p_{2nd}^h$)**.** *For a given function $U^* : \Omega \to \mathbb{R}^2$(or $\mathbb{R}^3$), let p be a solution to the 2-D (or 3-D) Poisson equation (4), and let p_{2nd}^h be the numerical solution of the second-order method (6). Then, the weighted discrete gradient has one and a half-order convergence in discrete L^2-norm:*

$$\|W^h G^h (p_{2nd}^h - p)\|_F \le C h^{3/2},$$

where the positive constant C depends only on the initial grid structure, U^*,and p^h.

Proof. In the estimate (9), the L^2-norm of $W^h G^h e_{2nd}^h$ is bounded as $\|W^h G^h e_{2nd}^h\|_F^2 \le \|d_{2nd}^h\|_F^2 + 2|\langle W^h d_{2nd}^h - d_{2nd}^h, G^h e_{2nd}^h\rangle_F|$. We use Lemma 6 to obtain

$$\begin{aligned}\|d_{2nd}^h\|_F^2 &= \sum_{A_{ij}:\text{uniform}} |d_{2nd,ij}^h|^2 \Delta_{ij} |A_{ij}| + \sum_{A_{ij}:\text{non-uniform}} |d_{2nd,ij}^h|^2 \Delta_{ij} |A_{ij}| \\ &\le C_1^2 h^6 (\#\text{ of uniform faces}) + C_2^2 h^4 (\#\text{ of non-uniform faces}).\end{aligned}$$

However, the number of uniform faces and non-uniform faces are bounded by

$$(\#\text{ of uniform faces}) \le C_3 h^{-2}, \quad (\#\text{ of non-uniform faces}) \le C_4 h^{-1},$$

where C_3 and C_4 are the constants only depend on the initial quadtree structure. Therefore, we estimate the L^2-norm of d^h as

$$\|d_{2nd}^h\|_F^2 \le C_1^2 C_3 h^4 + C_2^2 C_4 h^3.$$

On the other hand, we use Lemma 8 and Cauchy-Schwarz inequality to obtain

$$2|\langle W^h d_{2nd}^h - d_{2nd}^h, G^h e_{2nd}^h\rangle_F| \le \frac{1}{\delta}\|W^h d_{2nd}^h - d_{2nd}^h\|_F^2 + \delta \|G^h e_{2nd}^h\|_F^2 \le \frac{1}{\delta}\|d_{2nd}^h\|_F^2 + C_0 \delta \|W^h G^h e_{2nd}^h\|_F^2,$$

for any $\delta > 0$, where we use $\|d_{2nd}^h\|_F^2 = \|d_{2nd}^h - W^h d_{2nd}^h\|_F^2 + \|W^h d_{2nd}^h\|_F^2$. Combining the estimates, we obtain

$$\|W^h G^h e_{2nd}^h\|_F^2 \le \|d_{2nd}^h\|_F^2 + 2|\langle W^h d_{2nd}^h - d_{2nd}^h, G^h e_{2nd}^h\rangle_F| \le \left(1 + \frac{1}{\delta}\right)\left(C_1^2 C_3 h^4 + C_2^2 C_4 h^3\right) + C_0\delta \|W^h G^h e_{2nd}^h\|_F^2.$$

Now, we choose δ sufficiently small so that $C_0\delta < 1$. Then, we obtain

$$\|W^h G^h e_{2nd}^h\|_F^2 \le \frac{1 + \frac{1}{\delta}}{1 - C_0\delta}\left(C_1^2 C_3 h^4 + C_2^2 C_4 h^3\right) \le \frac{2(1+\delta)}{\delta(1 - C_0\delta)} C_2^2 C_4 h^3$$

for sufficiently small h. Therefore, taking $C := \sqrt{\frac{2(1+\delta)}{\delta(1-C_0\delta)} C_2^2 C_4}$, the desired one and a half order convergence of the discrete gradient holds. The octree case is similar with the proof of theorem 7. □

As corollaries of Theorem 7 and Theorem 9, we present the super-convergence of $G^h p_{1st}^h$ and $W^h G^h p_{2nd}^h$ toward the exact gradient $(\nabla p)^h$ where $(\nabla p)_{ij}^h := \sigma_{ij}(\nabla p)_{ij} \cdot n_{ij}$. Again, since the proofs are almost the same, we only present the proof for the second-order method.

Corollary 10. *For a given function $U^* : \Omega \to \mathbb{R}^2$ (or $\mathbb{R}^3$), let p be a solution to the 2-D (or 3-D) Poisson equation (4), and let p_{1st}^h be the numerical solution of the first-order method (3). Then,*

$$\|G^h p_{1st}^h - (\nabla p)^h\|_F \le C h^{1/2}.$$

Corollary 11. *For a given function $U^* : \Omega \to \mathbb{R}^2$ (or $\mathbb{R}^3$), let p be a solution to the 2-D (or 3-D) Poisson equation (4), and let p_{2nd}^h be the numerical solution of the second-order method* (6)*. Then,*

$$\|W^h G^h p_{2nd}^h - (\nabla p)^h\|_F \le C h^{3/2}.$$

Proof. Since $\|W^h G^h p_{2nd}^h - (\nabla p)^h\|_F \le \|W^h G^h p_{2nd}^h - W^h G^h p\|_F + \|W^h G^h p - (\nabla p)^h\|_F$, it suffice to estimate $\|W^h G^h p - (\nabla p)^h\|_F$. However, a similar estimate as in the proof of Lemma 6 implies that

$$|(W^h G^h p)_{ij} - (\nabla p)_{ij}^h| \le \begin{cases} C_5 h^2, & \text{if } A_{ij} \text{ is uniform,} \\ C_6 h, & \text{if } A_{ij} \text{ is non-uniform} \end{cases}$$

for some constants C_5 and C_6. Therefore, after the same argument in estimating the L^2-norm of d_{2nd}^h, we have $\|W^h G^h p - (\nabla p)^h\|_F^2 \le C_5^2 C_3 h^4 + C_6^2 C_4 h^3$. Therefore, combined with Theorem 9, we have the desired one and a half convergence estimate to exact gradient. □

4 Numerical results

In this section, we present numerical results to validate theories related to the super-convergences and stability in the Hodge decomposition. All the computations were implemented in C++, and conducted on a regular personal computer with a 3.60 GHz CPU and 16.0 GB memory. Every linear system $A^h p^h = (\nabla \cdot U^*)^h$ is solved by the Conjugate Gradient (CG) and the stopping criterion for CG is selected to be $\|r_n\| / \|r_0\| < 10^{-12}$.

4.1 Quadtree example

In this subsection, two dimensional example on the domain $\Omega = \left[-\frac{\pi}{2}, \frac{\pi}{2}\right]^2$ is considered to validate the results of corollaries 10 and 11. The original adaptive grid configuration based on the quadtree is depicted in figure 4 and the right hand side of the linear equation (4) is chosen by the divergence of the vector field $U^* = (u^*, v^*)$ where

$$u^*(x, y) = -\cos(x)\sin(y) + \frac{1}{2}\sin(2x)$$
$$v^*(x, y) = \sin(x)\cos(y) + \frac{1}{2}\sin(2y)$$

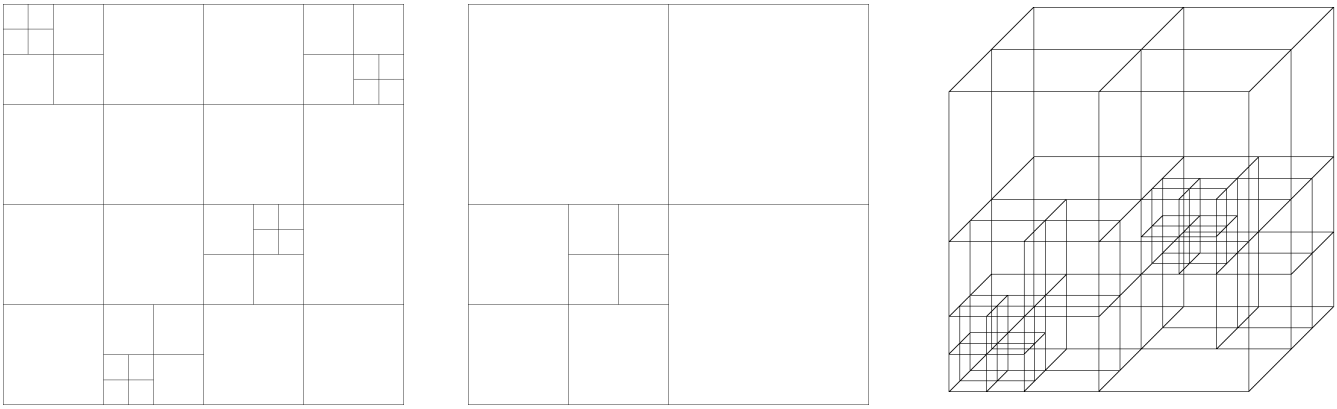

(a) (b) (c)

Figure 4: Original adaptive grids for the numerical examples in section 4. The two dimensional grid configurations (a) and (b) for a domain $\Omega = \left[-\frac{\pi}{2}, \frac{\pi}{2}\right]^2$ are selected for examples in section 4.1 and 4.3, respectively, and the three dimensional configuration (c) for a domain $\Omega = \left[-\frac{\pi}{2}, \frac{\pi}{2}\right]^3$ is chosen for the example in section 4.2.

Effective resolution	$\left\|G^h p^h_{1st} - (\nabla p)^h\right\|_F$	order	$\left\|W^h G^h p^h_{2nd} - (\nabla p)^h\right\|_F$	order
32^2	0.188413		0.037916	
64^2	0.134469	0.486625	0.013216	1.520521
128^2	0.095886	0.487882	0.004528	1.54534
256^2	0.068184	0.491887	0.001556	1.541032
512^2	0.048374	0.495201	0.000539	1.529485
1024^2	0.034270	0.497286	0.000188	1.519553

Table 1: (Quadtree example) The rates of $\left\|G^h p^h_{1st} - (\nabla p)^h\right\|_F$ and $\left\|W^h G^h p^h_{2nd} - (\nabla p)^h\right\|_F$ are 0.5 and 1.5, validating corollaries 10 and 11, respectively.

so that the solution of system (4) is $p(x, y) = -\frac{1}{4}(\cos(2x) + \cos(2y))$.

Numerical results based on the first-order [9] and second-order [8] discretizations are reported in table 1. The results verify that the half order accuracy for [9] and the one and a half order accuracy for [8] in the solution's gradient in L^2-norm, which agree with corollaries 10 and 11. Figure 5 presents the profiles (log scale) of the L^2-error of gradients $\left\|W^h G^h p^h_{2nd} - (\nabla p)^h\right\|_F$ and the number $Ch^{\frac{3}{2}}$, as in the proof of corollary 11, with respect to the largest cell size h.

4.2 Octree example

Consider a domain $\Omega = \left[-\frac{\pi}{2}, \frac{\pi}{2}\right]^3$and a vector field $U^* = (u^*, v^*, w^*)$ for the system (4) as follow:

$$u^*(x, y, z) = -2\cos(x)\sin(y)\sin(z) + \frac{1}{2}\sin(2x)$$
$$v^*(x, y, z) = \sin(x)\cos(y)\sin(z) + \frac{1}{2}\sin(2y)$$
$$w^*(x, y, z) = \sin(x)\sin(y)\cos(z) + \frac{1}{2}\sin(2z).$$

In order to validate the results of corollaries 10 and 11, the linear systems (3) and (6) are solved in the domain depicted in the figure 4.

Table 2 shows the convergence orders of $\left\|G^h p^h_{1st} - (\nabla p)^h\right\|_F$ and $\left\|W^h G^h p^h_{2nd} - (\nabla p)^h\right\|_F$, where p is given by $p(x, y, z) = -\frac{1}{4}(\cos(2x) + \cos(2y) + \cos(2z))$. The results demonstrate that our analyses given in corollaries 10

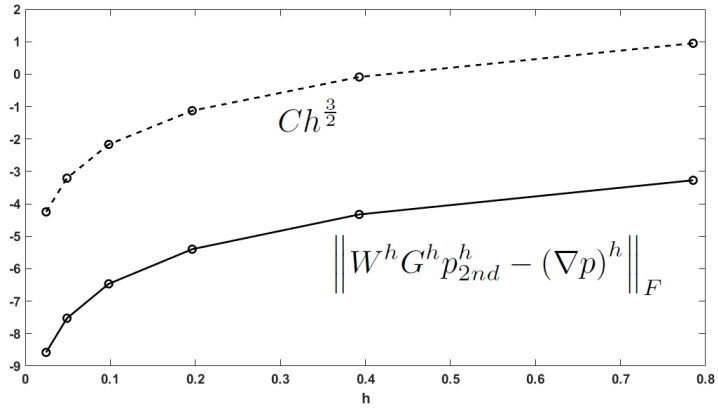

Figure 5: (Quadtree example) Plots (log scale) of L^2-error of the discrete gradient $\left\|W^h G^h p^h_{2nd} - (\nabla p)^h\right\|_F$ and an upper bound $Ch^{\frac{3}{2}}$ where C is the constant in the proof of corollary 11 for the example in section 4.1. Numerical results show that $\left\|W^h G^h p^h_{2nd} - (\nabla p)^h\right\|_F$ is bounded above by $Ch^{\frac{3}{2}}$, which means the discrete gradient has one and a half-order convergence in discrete L^2-norm.

Effective resolution	$\left\|G^h p^h_{1st} - (\nabla p)^h\right\|_F$	order	$\left\|W^h G^h p^h_{2nd} - (\nabla p)^h\right\|_F$	order
16^3	0.504592		0.258934	
32^3	0.350232	0.526806	0.084916	1.608476
64^3	0.248422	0.495518	0.028619	1.569063
128^3	0.176518	0.492978	0.009859	1.53746
256^3	0.123283	0.517841	0.003459	1.511086

Table 2: (Octree example) The rates of $\left\|G^h p^h_{1st} - (\nabla p)^h\right\|_F$ and $\left\|W^h G^h p^h_{2nd} - (\nabla p)^h\right\|_F$ are 0.5 and 1.5, validating corollaries 10 and 11, respectively.

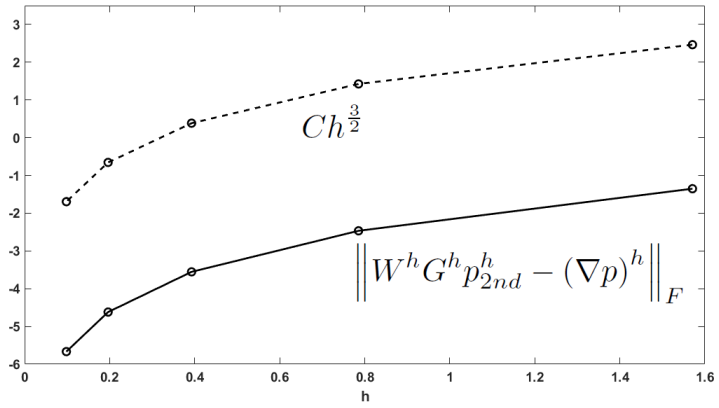

Figure 6: (Octree example) Plots (log scale) of L^2-error of the discrete gradient $\left\|W^h G^h p^h_{2nd} - (\nabla p)^h\right\|_F$ and an upper bound $Ch^{\frac{3}{2}}$ where C is the constant in the proof of corollary 11 for the example in section 4.1. Numerical results show that $\left\|W^h G^h p^h_{2nd} - (\nabla p)^h\right\|_F$ is bounded above by $Ch^{\frac{3}{2}}$, which means the discrete gradient has one and a half-order convergence in discrete L^2-norm.

and 11 are valid for the octree-based grid configuration. The profiles in figure 6 support the convergence anaylsis in corollary 11.

4.3 Single vortex in two spatial dimensions

In this subsection, we consider the following incompressible inviscid Navier-Stokes equations

$$\begin{cases} \frac{\partial U}{\partial t} + (U \cdot \nabla) U & = -\nabla p + F \\ \nabla \cdot U & = 0 \end{cases}. \tag{10}$$

Here, U is the fluid velocity, p is the pressure, and F is the acceleration by external force. One of the typical method to solve (10) is the projection method [2], which is a splitting-type method based on the Hodge decomposition. The method first computes an intermediate velocity U^* without the presure term, that is,

$$\frac{U^* - U^n}{\Delta t} + (U^n \cdot \nabla) U^n = F^n. \tag{11}$$

As a second step, the method computes the velocity U^{n+1} only with the pressure term by enforcing the incompressibility as follow

$$\begin{cases} \frac{U^{n+1} - U^*}{\Delta t} & = -\nabla p^{n+1} \\ \nabla \cdot U^{n+1} & = 0 \end{cases} \tag{12}$$

which leads to the Poisson equation (4) with Neumann boundary conditions.

In order to valdiate the stability on the Hodge projection, stated in proposition 4, we consider an inviscid single vortex flow in a two dimensional domain $\Omega = \left[-\frac{\pi}{2}, \frac{\pi}{2}\right]^2$ with the velocity $U = (u, v)$ and p are given by

$$\begin{aligned} u(x, y, t) &= -\cos(x) \sin(y) \cos(t) \\ v(x, y, t) &= \sin(x) \cos(y) \cos(t) \\ p(x, y, t) &= 0.5 \left(\cos^2(x) + \cos^2(y)\right) \cos^2(t), \end{aligned}$$

and the forcing term F is calculated from the above formulae and equation (10). The first step (11) of the projection method is simply solved by the semi-Lagrangian method as follow

$$\frac{U^* - U_d}{\Delta t} = F^n,$$

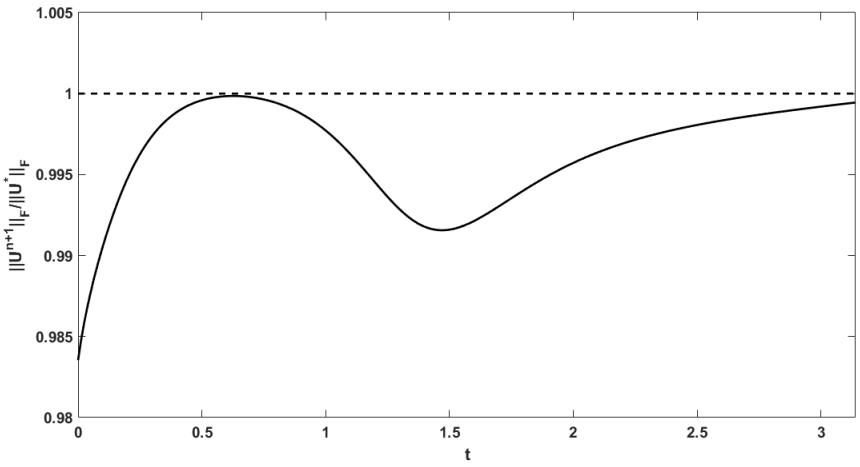

Figure 7: The ratio $\left\|U_{2nd}^{n+1}\right\|_F / \|U^*\|_F$ for the inviscid single vortex flow in section 4.3. The result shows that the ratio $\left\|U_{2nd}^{n+1}\right\|_F / \|U^*\|_F$ is bounded above by 1, that is, $\left\|U_{2nd}^{n+1}\right\|_F \leq \|U^*\|_F$. This agrees with the result of proposition 4.

where $U_d = U^n\left(x - u^n\Delta t, y - v^n\Delta t\right)$ is the semi-Lagrangian [4] approximated velocity with RBF [5] interpolation. The original adaptive grid configuration for the simulation is depicted in figure 4 and effective resolution for the simulation is selected so that $h = \Delta x = \Delta y = \frac{\pi}{64}$ with $\Delta t = \Delta x/2$.

Figure 7 shows the ratio between $\left\|U_{2nd}^{n+1}\right\|_F$ and $\|U^*\|_F$, which demonstrates that the Hodge decomposition with the linear solver (6) is stable in the sense that $\left\|U_{2nd}^{n+1}\right\|_F \leq \|U^*\|_F$.

5 Conclusion

We noted the importance of symmetry in the Poisson solvers by Losasso et al. [9, 8]. The symmetry is a necessary condition of the minimization property, and numerical solutions of the solvers are desired to satisfy the minimization property for the stability when they incorporate with the Hodge decomposition in simulating incompressible fluid flows. We showed in section 2 that the Poisson solvers indeed satisfy the minimization properties in discrete level and presented numerical results in section 4 which validate the stability in solving incompressible fluid flows.

Furthermore, we presented rigorous analyses for the super-convergences of numerical solutions p_{1st} and p_{2nd} of the 1st-order [9] and 2nd-order [8] solvers, respectively, in section 3. The common strategy for the analyses is to express the consistency errors as the divergence forms, introduced in [16], but it turns out to be applicable only for the 1st-order method. In order to prove the super-convergence for the 2nd-order method, we note that the 2nd-order method can be seen as the weighted average of the 1st-order method. Based on this observation, we found out the L^2 norm estimation of the symmetric operator W^h in lemma 8, which enables us to prove the super-convergence for the 2nd-order method. All the analyses are not only valid for the quadtree but also for the octree configuration. Numerical results in section 4 support the analyses, and suggest that our estimates are tight.

Acknowledgement

The research of Byungjoon Lee was supported by the Catholic University of Korea, Research Fund, 2020 and NRF grant 2020R1A2C4002378. The research of Jeongho Kim was supported by the Basic Science Research Program through the National Research Foundation of Korea(NRF) funded by the Ministry of Science and ICT (NRF-2020R1A4A3079066). The research of Chohong Min was supported by Basic Science Research Program through the National Research Foundation of Korea(NRF) funded by the Ministry of Education (Grant No. 2019R1A6A1A11051177 and 2021R1A2C1095703).

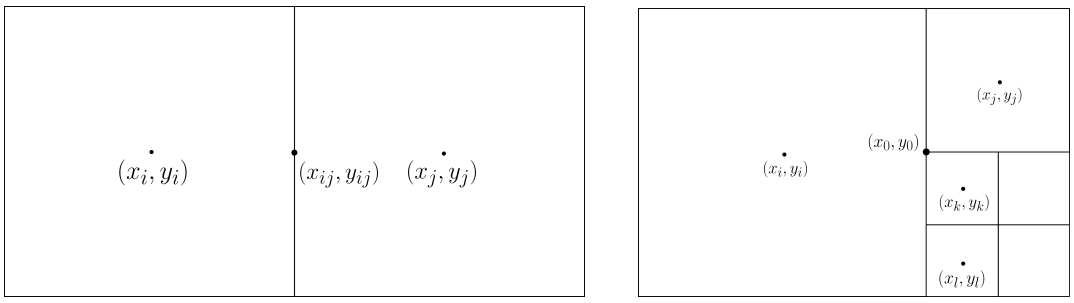

Figure 8: Structures of uniform face (Left) and non-uniform face (Right).

Appendix

In this appendix, we present the detailed proofs of Lemma 6 and Lemma 8.

Proof of Lemma 6

Proof. For simplicity, we refer $d^h_{2nd,ij}$ as d^h_{ij}. First, we split $|d^h_{ij}|$ into two terms I_1 and I_2 as

$$|d^h_{ij}| \le \left|(W^h U^{*,h})_{ij} - (S^h U^*)_{ij}\right| + \left|(S^h \nabla p)_{ij} - (W^h G^h p)_{ij}\right| = I_1 + I_2.$$

Below, we estimate each term I_1 and I_2, according to the type of face A_{ij}.

• Case 1 (A_{ij} is uniform): We first consider the case when A_{ij} is uniform, as it is illustrated in Figure 8 (Left). Then, we have $(W^h U^{*,h})_{ij} = U^{*,h}_{ij}$ and $(W^h G^h p)_{ij} = (G^h p)_{ij}$. Furthermore, we assume that A_{ij} is a vertical face. Let (x_i, y_i),(x_j, y_j) be the cooridnates of centers of the cells C_i and C_j and (x_{ij}, y_{ij}) be the coordinate of center of the face A_{ij}. Since the cells C_i and C_j have the same size, we have $|A_{ij}| = \Delta_{ij} = |x_j - x_i| \le h$, and $n_{ij} = (\pm 1, 0)$. We use Taylor theorem to u^*,where $U^* = (u^*, v^*)$, to estimate u^* on the face A_{ij} as

$$u^*(x_{ij}, y) = u^*_{ij} + u^*_y(x_{ij}, y_{ij})(y - y_{ij}) + \frac{u^*_{yy}(x_{ij}, \hat{y}_{ij})}{2}(y - y_{ij})^2, \quad y \in \left[y_{ij} - \frac{|A_{ij}|}{2}, y_{ij} + \frac{|A_{ij}|}{2}\right]$$

for some $\hat{y}_{ij}$ between y and y_{ij}. Therefore, we estimate I_1 as

$$\begin{aligned} I_1 &= |u^*_{ij} - (S^h U^*)_{ij}| \\ &= \frac{1}{|A_{ij}|}\left|\int_{y_{ij} - \frac{|A_{ij}|}{2}}^{y_{ij} + \frac{|A_{ij}|}{2}} u^*_y(x_{ij}, y_{ij})(y - y_{ij}) + \frac{u^*_{yy}(x_{ij}, \hat{y}_{ij})}{2}(y - y_{ij})^2\, dy\right| \\ &\le \frac{\|u^*_{yy}\|_{L^\infty}}{24}|A_{ij}|^2 \le \frac{\|u^*_{yy}\|_{L^\infty}}{24}h^2. \end{aligned}$$

In order to estimate I_2, we again use Taylor theorem to p to obtain

$$\begin{aligned} p_j &= p(x_{ij}, y_{ij}) + p_x(x_{ij}, y_{ij})(x_j - x_{ij}) + \frac{p_{xx}(x_{ij}, y_{ij})}{2}(x_j - x_{ij})^2 + \frac{p_{xxx}(\hat{x}_{ij}, y_{ij})}{6}(x_j - x_{ij})^3, \\ p_i &= p(x_{ij}, y_{ij}) + p_x(x_{ij}, y_{ij})(x_i - x_{ij}) + \frac{p_{xx}(x_{ij}, y_{ij})}{2}(x_i - x_{ij})^2 + \frac{p_{xxx}(\tilde{x}_{ij}, y_{ij})}{6}(x_i - x_{ij})^3, \end{aligned}$$

for some $\hat{x}_{ij}, \tilde{x}_{ij}$ between x_j, x_i and x_{ij}. We use $|x_i - x_{ij}| = |x_{ij} - x_j| = \frac{\Delta_{ij}}{2}$ and $x_j - x_i = \sigma_{ij}\Delta_{ij}$to derive

$$\frac{p_j - p_i}{\Delta_{ij}} = \sigma_{ij} p_x(x_{ij}, y_{ij}) - \sigma_{ij}\frac{p_{xxx}(\hat{x}_{ij}, y_{ij}) + p_{xxx}(\tilde{x}_{ij}, y_{ij})}{48}\Delta^2_{ij},$$

which implies

$$\left|p_x(x_{ij}, y_{ij}) - (G^h p)_{ij}\right| \leq \frac{\|p_{xxx}\|_{L^\infty}}{24}\Delta_{ij}^2.$$

Then, we estimate I_2 as

$$\begin{aligned} I_2 = \left|(S^h\nabla p)_{ij} - (G^h p)_{ij}\right| &\leq \left|(S^h\nabla p)_{ij} - p_x(x_{ij}, y_{ij})\right| + \left|p_x(x_{ij}, y_{ij}) - (G^h p)_{ij}\right| \\ &\leq \frac{\|\nabla p_{yy}\|_{L^\infty}}{24}h^2 + \frac{\|p_{xxx}\|_{L^\infty}}{24}h^2, \end{aligned}$$

where the estimate of the first term can be obtained by using exactly the same argument as in the estimate of I_1. Combining the estimates for I_1 and I_2, $|d_{ij}^h|$ is bounded as

$$|d_{ij}^h| \leq I_1 + I_2 \leq \frac{h^2}{24}\left(\|u_{yy}^*\|_{L^\infty} + \|\nabla p_{yy}\|_{L^\infty} + \|p_{xxx}\|_{L^\infty}\right),$$

The case when A_{ij} is a horizontal unfiorm face can be estimated in the same manner, and therefore, when A_{ij} is uniform, we have $|d_{ij}^h| \leq C_1 h^2$, with

$$C_1 := \frac{1}{24}\max\left\{\|u_{yy}^*\|_{L^\infty} + \|\nabla p_{yy}\|_{L^\infty} + \|p_{xxx}\|_{L^\infty}, \|v_{xx}^*\|_{L^\infty} + \|\nabla p_{xx}\|_{L^\infty} + \|p_{yyy}\|_{L^\infty}\right\}.$$

• Case 2 (A_{ij} is non-uniform): We now consider the case when A_{ij} is non-uniform as in Figure 8 (Right). Again, we assume that A_{ij} is a vertical face. Suppose the cell C_j is smaller than the cell $C_i$and let A_i be the edge of the cell C_i that is adjacent to cell C_j. Let $\{C_k\}$ be all the cells that are adjacent to C_i through the large face A_i and let (x_0, y_0) be the coordinate of the center of the A_i. First, we note that for $y \in [y_0, y_0 + |A_{ij}|]$,

$$|u_{ik}^* - u^*(x_0, y)| \leq \|u_y^*\|_{L^\infty} h.$$

Therefore, we estimate I_1 as

$$I_1 = \left|(W^h U^{*,h})_{ij} - (S^h U^*)_{ij}\right| \leq \frac{1}{|A_{ij}|}\int_{A_{ij}} \|u_y^*\|_{L^\infty} h\, dy \leq \|u_y^*\|_{L^\infty} h.$$

In order to estimate I_2, we further split it into two parts as

$$I_2 \leq \left|(S^h\nabla p)_{ij} - p_x(x_0, y_0)\right| + \left|p_x(x_0, y_0) - (W^h G^h p)_{ij}\right|.$$

Using a similar argument as in the estimate of I_1, the first term can be easily estimated as

$$\left|(S^h\nabla p)_{ij} - p_x(x_0, y_0)\right| \leq \frac{\|p_{xy}\|_{L^\infty}}{2}h.$$

To estimate the second term, we use Taylor theorem at (x_0, y_0) to obtain

$$\begin{aligned} p_k &= p(x_0, y_0) + p_x(x_0, y_0)(x_k - x_0) + p_y(x_0, y_0)(y_k - y_0) + R_k, \\ p_i &= p(x_0, y_0) + p_x(x_0, y_0)(x_i - x_0) + R_i, \end{aligned}$$

where the remainder terms are estimated as $|R_i|, |R_k| \leq \frac{|x_i - x_0|^2}{2}\|\nabla^2 p\|_{L^\infty}$. Therefore, we have

$$(W^h G^h p)_{ij} = \frac{\sum_k (p_x(x_0, y_0)(x_k - x_i) + p_y(x_0, y_0)(y_k - y_0) + (R_k - R_i))\sigma_{ik}|A_{ik}|}{\sum_k \Delta_{ik}|A_{ik}|}.$$

However, it follows from the quadtree structure that

$$\sum_k (x_k - x_i)\sigma_{ik}|A_{ik}| = \sum_k \Delta_{ik}|A_{ik}|, \quad \sum_k (y_k - y_0)|A_{ik}| = 0.$$

Hence, the discrete gradient can be estimated as

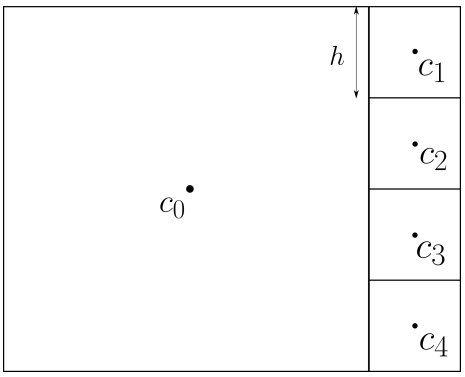

Figure 9: An example cell structure for Lemma 6. All the four adjacent cells are of the same size.

$$|p_x(x_0,y_0) - (W^h G^h p)_{ij}| \le \frac{|x_i - x_0|^2 |A_i|}{\sum_k \Delta_{ik}|A_{ik}|} \|\nabla^2 p\|_{L^\infty} \le |x_i - x_0| \|\nabla^2 p\|_{L^\infty} \le \frac{\|\nabla^2 p\|_{L^\infty}}{2} h.$$

Therefore, we yield the following bound for I_2:

$$I_2 \le \frac{\|p_{xy}\|_{L^\infty}}{2} h + \frac{\|\nabla^2 p\|_{L^\infty}}{2} h \le \|\nabla^2 p\|_{L^\infty} h.$$

We combine the estimates for I_1 and I_2 to estimate $|d_{ij}^h|$ as

$$|d_{ij}^h| \le I_1 + I_2 \le h(\|u_y^*\|_{L^\infty} + \|\nabla^2 p\|_{L^\infty}).$$

Therefore, for any non-uniform face A_{ij}, we have $|d_{ij}^h| \le C_2 h$, where $C_2 := \max\{\|u_x^*\|_{L^\infty}, \|u_y^*\|_{L^\infty}\} + \|\nabla^2 p\|_{L^\infty}$. □

Proof of Lemma 8

Proof. First of all, we note that W^h is a local operator, since it returns a weighted average among the faces that are included in a common large face. Therefore, it suffice to show that the desired inequality holds for a single large face. Furthermore, we note that the cells that are adjacent to a common large cell have the same size, after successive refinements. Therefore, we only need to show that the inequality holds for the cell structure where all the small cells that are adjacent to a common large cell have the same size. For example, consider the cell structure in Figure 9.

Among the terms in L^2-norm of $G^h c^h$, the terms correspond to the cell structure in Figure 9 is given as

$$I_1 := ((G^h c^h)_{01}^2 + (G^h c^h)_{02}^2 + (G^h c^h)_{03}^2) + (G^h c^h)_{04}^2) 2.5h^2 + ((G^h c^h)_{12}^2 + (G^h c^h)_{23}^2 + (G^h c^h)_{34}^2) h^2.$$

The aim is to bound by a constant multiple of the following quantity:

$$I_2 := (W^h G^h c^h)_{01}^2 10h^2 + ((W^h G^h c^h)_{12}^2 + (W^h G^h c^h)_{23}^2 + (W^h G^h c^h)_{34}^2) h^2,$$

where we used $(W^h G^h c^h)_{01} = (W^h G^h c^h)_{02} = (W^h G^h c^h)_{03} = (W^h G^h c^h)_{04}$. We rewrite $(G^h c^h)_{01}$ as

$$\begin{aligned}
(G^h c^h)_{01} &= \frac{c_1 - c_0}{2.5h} = \frac{\frac{c_1+c_2+c_3+c_4}{4} - c_0}{2.5h} + \frac{(c_1 - c_2) + (c_1 - c_3) + (c_1 - c_4)}{10h} \\
&= (W^h G^h c^h)_{01} + \frac{3}{10}\frac{c_1 - c_2}{h} + \frac{2}{10}\frac{c_2 - c_3}{h} + \frac{1}{10}\frac{c_3 - c_4}{h} \\
&= (W^h G^h c^h)_{01} + \frac{3}{10}(W^h G^h c^h)_{12} + \frac{2}{10}(W^h G^h c^h)_{23} + \frac{1}{10}(W^h G^h c^h)_{34}.
\end{aligned}$$

n	1	2	3	4	5	6
$\lambda_{\max}$	$\frac{4}{3}$	1.6828	2.4597	4.0614	7.2931	13.7722

Table 3: The maximum eigenvalues of $A^\top A$ according to the cell structure with 2^n small cells in the proof of lemma 8. A cell has 2^n number of adjacent cells on one face as in figure 9. The constant C_0 in the lemma equals to $\lambda_{\max}(A^\top A)$.

Similarly, the other gradients can be written as

$$
\begin{aligned}
(G^h c^h)_{02} &= (W^h G^h c^h)_{02} - \frac{1}{10}(W^h G^h c^h)_{12} + \frac{2}{10}(W^h G^h c^h)_{23} + \frac{1}{10}(W^h G^h c^h)_{34},\\
(G^h c^h)_{03} &= (W^h G^h c^h)_{03} - \frac{1}{10}(W^h G^h c^h)_{12} - \frac{2}{10}(W^h G^h c^h)_{23} + \frac{1}{10}(W^h G^h c^h)_{34},\\
(G^h c^h)_{04} &= (W^h G^h c^h)_{04} - \frac{1}{10}(W^h G^h c^h)_{12} - \frac{2}{10}(W^h G^h c^h)_{23} - \frac{3}{10}(W^h G^h c^h)_{34}.
\end{aligned}
$$

On the other hand, since $(G^h c^h)_{12} = (W^h G^h c^h)_{12}, (G^h c^h)_{23} = (W^h G^h c^h)_{23}$, and $(G^h c^h)_{34} = (W^h G^h c^h)_{34}$, we have,

$$
\begin{bmatrix}
\sqrt{2.5}(G^h c^h)_{01}\\
\sqrt{2.5}(G^h c^h)_{02}\\
\sqrt{2.5}(G^h c^h)_{03}\\
\sqrt{2.5}(G^h c^h)_{04}\\
(G^h c^h)_{12}\\
(G^h c^h)_{23}\\
(G^h c^h)_{34}
\end{bmatrix}
=
\underbrace{\begin{bmatrix}
\frac{1}{4} & \frac{3\sqrt{2.5}}{10} & \frac{2\sqrt{2.5}}{10} & \frac{\sqrt{2.5}}{10}\\
\frac{1}{4} & -\frac{\sqrt{2.5}}{10} & \frac{2\sqrt{2.5}}{10} & \frac{\sqrt{2.5}}{10}\\
\frac{1}{4} & -\frac{\sqrt{2.5}}{10} & -\frac{2\sqrt{2.5}}{10} & \frac{\sqrt{2.5}}{10}\\
\frac{1}{4} & -\frac{\sqrt{2.5}}{10} & -\frac{2\sqrt{2.5}}{10} & -\frac{3\sqrt{2.5}}{10}\\
0 & 1 & 0 & 0\\
0 & 0 & 1 & 0\\
0 & 0 & 0 & 1
\end{bmatrix}}_{=:A}
\begin{bmatrix}
\sqrt{10}(W^h G^h c^h)_{01}\\
(W^h G^h c^h)_{12}\\
(W^h G^h c^h)_{23}\\
(W^h G^h c^h)_{34}
\end{bmatrix}.
$$

Then, considering the quadratic structures of I_1 and I_2, we have $I_1 \le \lambda_{\max}(A^\top A) I_2$,where the maximum eigenvalue of $A^\top A$ is given as $\frac{7+\sqrt{2}}{5} \approx 1.6828$. Since the type of the cell structure is completely determined by the initial quadtree structure, there exists a positive constant C_0 such that $\|G^h c^h\|_{2,F}^2 \le C_0 \|W^h G^h c^h\|_{2,F}^2$, where C_0 only depends on the initial quadtree structure. For reference, we provide the maximum eigenvalue $\lambda_{\max}(A^\top A)$ when there exist 2^n cells adjacent to a common large cell in Table 3. □

Remark 12. For the case of Octree grid, it suffice to consider the case when there exist 4^n cells adjacent to a common large cell, by the same reason as in the Quadtree grid. In such case, the maximum eigenvalues $\lambda_{\max}(A^\top A)$ can be estimated as $\frac{5+\sqrt{2}}{3} \approx 2.1381...$ for $n = 1$ and 5.0655... for $n = 2$.

References

[1] Christopher Batty, Florence Bertails, and Robert Bridson. A fast variational framework for accurate solid-fluid coupling. *ACM Transactions on Graphics (TOG)*, 26(3):100–107, 2007.

[2] Alexandre Joel Chorin. The numerical solution of the navier-stokes equations for an incompressible fluid. *Bulletin of the American Mathematical Society*, 73(6):928–931, 1967.

[3] Philippe G. Ciarlet. *The finite element method for elliptic problems*. SIAM, 2002.

[4] Richard Courant, Eugene Isaacson, and Mina Rees. On the solution of nonlinear hyperbolic differential equations by finite differences. *Communications on pure and applied mathematics*, 5(3):243–255, 1952.

[5] Rolland L. Hardy. Multiquadric equations of topography and other irregular surfaces. *Journal of geophysical research*, 76(8):1905–1915, 1971.

[6] Kwang-Yeon Kim. Robust a posteriori error estimator for lowest-order finite element methods of interface problems. *Journal of the Korean Society for Industrial and Applied Mathematics*, 20(2):137–150, 2016.

[7] Qun Lin, Lutz Tobiska, and Aihui Zhou. Superconvergence and extrapolation of non-conforming low order finite elements applied to the poisson equation. *IMA Journal of Numerical Analysis*, 25(1):160–181, 2005.

[8] Frank Losasso, Ronald Fedkiw, and Stanley Osher. Spatially adaptive techniques for level set methods and incompressible flow. *Computers & Fluids*, 35(10):995–1010, 2006.

[9] Frank Losasso, Frédéric Gibou, and Ronald Fedkiw. Simulating water and smoke with an octree data structure. In *ACM SIGGRAPH 2004 Papers*, pages 457–462. 2004.

[10] Chohong Min, Frédéric Gibou, and Hector D. Ceniceros. A supra-convergent finite difference scheme for the variable coefficient poisson equation on non-graded grids. *Journal of Computational Physics*, 218(1):123–140, 2006.

[11] Stéphane Popinet. An accurate adaptive solver for surface-tension-driven interfacial flows. *Journal of Computational Physics*, 228(16):5838–5866, 2009.

[12] James W. Purvis and John E. Burkhalter. Prediction of critical mach number for store configurations. *AIAA Journal*, 17(11):1170–1177, 1979.

[13] Yousef Saad. *Iterative methods for sparse linear systems*. SIAM, 2003.

[14] John C. Strikwerda. *Finite difference schemes and partial differential equations*. SIAM, 2004.

[15] Steven R. White, John W. Wilkins, and Michael P. Teter. Finite-element method for electronic structure. *Physical Review B*, 39(9):5819, 1989.

[16] Gangjoon Yoon, Jea-Hyun Park, and Chohong Min. Convergence analysis on the gibou–min method for the hodge projection. *Communications in Mathematical Sciences*, 15(5):1211–1220, 2017.